Thin-Walled Structures 48 (2010) 33–41

Contents lists available at ScienceDirect

Thin-Walled Structures

journal homepage: www.elsevier.com/locate/tws

Simplified models for cross-section stress demands on C-section purlins in uplift

L.C.M. Vieira Jr.[a,*,1], M. Malite[b], B.W. Schafer[a]

[a] Johns Hopkins University, Baltimore, MD, USA
[b] Universidade de São Paulo—EESC, São Carlos, SP, Brazil

ARTICLE INFO

Article history:
Received 6 March 2009
Received in revised form
19 June 2009
Accepted 20 July 2009
Available online 20 August 2009

Keywords:
Cold-formed steel
Purlins in uplift
Purlin-sheeting systems

ABSTRACT

The objective of this paper is to provide and verify simplified models that predict the longitudinal stresses that develop in C-section purlins in uplift. The paper begins with the simple case of flexural stress; where the force has to be applied at the shear center, or the section braced in both flanges. Restrictions on load application point and restraint of the flanges are removed until arriving at the more complex problem of bending when movement of the tension flange alone is restricted, as commonly found in purlin-sheeting systems. Winter's model for predicting the longitudinal stresses developed due to direct torsion is reviewed, verified, and then extended to cover the case of a bending member with tension flange restraint. The developed longitudinal stresses from flexure and restrained torsion are used to assess the elastic stability behavior of typical purlin-sheeting systems. Finally, strength predictions of typical C-section purlins are provided for existing AISI methods and a newly proposed extension to the direct strength method that employs the predicted longitudinal stress distributions within the strength prediction.

1. Introduction

The primary concern with cold-formed steel cross-sections is that due to their thin-walled nature instability phenomena must be examined, including but not limited to: local, distortional, and global buckling modes. Further, due to their lack of symmetry (i.e., commonly used C- and Z-section members are singly- and point-symmetric respectively) an additional issue is that even for common applications, operating in the elastic range, the sections may develop a complicated stress response, where conventional flexure theory (i.e., $\sigma = My/I$) approximations are grossly inadequate.

A common cold-formed steel application that leads to complicated stress response is the use of C-sections as purlins in metal building roofs, as shown in Fig. 1 (e.g., this is the common metal building roof system in Brazil). In uplift, the purlins tend to twist resulting in the addition of longitudinal stresses due to partially restrained warping torsion in addition to conventional bending stress. This paper provides an examination of these stresses, as well as the means to predict their magnitudes in design situations, and to determine their influence on elastic stability and strength.

Given that longitudinal stresses are known to have a significant impact on cross-section stability and strength, in the second part of this paper we examine the application of these stresses to strength prediction. The prediction methods examined include: (a) simple "R" factor reductions as found in D6.1.1 of AISI-S100-07 [1], (b) the application of the new torsion provisions as found in C3.6 of AISI-S100-07 [1], and (c) a novel extension to the direct strength method (DSM) of Appendix 1 of AISI-S100-07 [1,2] which uses the predicted stress demands to assess the local, distortional, and global stability and strength of the section directly.

It is worthy of noting that existing research on cold-formed steel purlins and purlin-sheeting systems is extensive. Including the recent work by Tom Murray and his students on anchorage forces [4,5] the extensive studies by Hancock and his students and colleagues including vacuum testing and the examination of rational elastic buckling analysis in design [6–10] as well as earlier theoretical and experimental work [11,12] to name but a few.

2. Cross-sections studied

The basic system studied in this paper is that of Fig. 1. The cross-section dimensions for the purlins are provided in Table 1. For the trapezoidal sheeting (height = 25 mm, $t = 0.43$ mm) shell element based finite element models were utilized to determine the rotational stiffness, k_{rx}, that the sheeting provides to the purlin, the resulting k_{rx} are provided in Table 1 [13]. Span lengths

* Corresponding author.
E-mail address: luizvieirajr@gmail.com (L.C.M. Vieira Jr.).
[1] Formerly graduate student Universidade de São Paulo—EESC, Brazil.

0263-8231/$ - see front matter © 2009 Elsevier Ltd. All rights reserved.
doi:10.1016/j.tws.2009.07.009

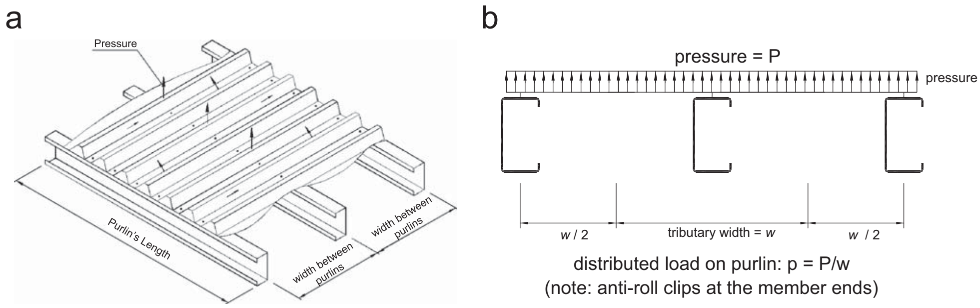

Fig. 1. Purlin-sheeting system under uplift ((a)–based on [3]): (a) isometric and (b) elevation with load from fasteners.

Table 1
Cross-section and rotational spring stiffness.

Section	$C{-}b_w \times b_f \times d \times t$	k_{rx} (kN. m/rad/m)
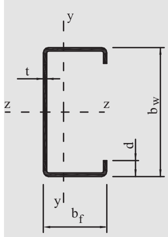	$150 \times 60 \times 20 \times 1.5$	0.39
	$200 \times 75 \times 20 \times 2$	0.58
	$250 \times 85 \times 25 \times 2$	0.68
	$250 \times 85 \times 25 \times 3$	0.72

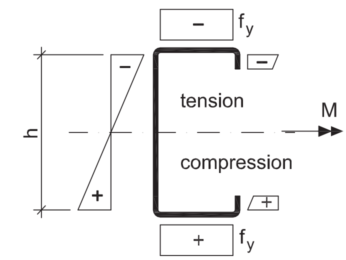

Fig. 3. Simple flexural stress.

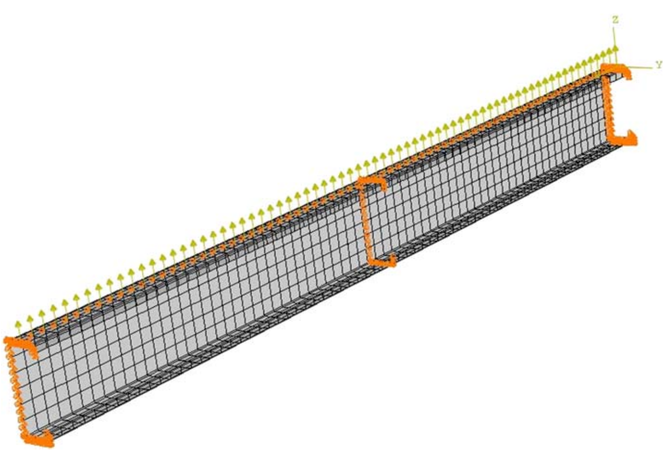

Fig. 2. Typical shell element model of bare purlin with uplift load.

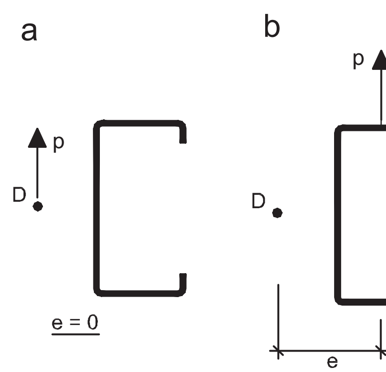

Fig. 4. Load application points: (a) load applied at shear center and (b) load applied at connection.

vary depending on the cross-section (see Table 1) but in general vary from 5 to 10 m. Additional material properties assumed include $E = 205{,}000$ MPa, $F_y = 300$ MPa, and $\nu = 0.3$.

A typical shell element model used for determination of the stress demands is shown in Fig. 2.

3. Fully braced: longitudinal stress demands

In the ideal fully braced case the behavior of a C-section purlin is well described by simple flexural stresses ($\sigma = My/I$), as shown in Fig. 3. For stresses to develop in this manner the section must be fully restrained from lateral translation and twist (or be loaded at its shear center). The restraint must be provided in such a manner that the section does not distort due to the bracing forces. Some form of blocking accompanied by attachments to both flanges is known to provide such adequate restraint.

4. Unbraced: longitudinal stress demands

For singly-symmetric sections, such as a C-section, it is well known that vertical loads must be applied at the shear center (Fig. 4a) if torsion is to be avoided. However, under uplift in a purlin the load path requires that the force be transmitted through the fastener, at mid-width of the flange, considerably away from the shear center.

The longitudinal stresses developed in pure bending (Fig. 4a) are compared with those including bending and torsion (of Fig. 4b) in Fig. 5, for the same load, p. In Fig. 5, σ_M refers to the longitudinal stresses from pure bending moment "M" and σ_B refers to the longitudinal stresses from the warping torsion bimoment "B" from Vlasov's theory [14] (at mid-length). As Fig. 5 indicates the introduction of warping torsion, and associated bimoment, radically alter the applied stress distribution on the section, net compressive stresses even end up on the "tension" flange (and vice-a-versa).

5. Unbraced: Winter's model for warping torsion stress

Calculation of the longitudinal warping stresses due to torsion by Vlasov's theory is involved; fortunately, Winter [15] developed an accurate approximate method that is fully illustrated in AISI (2004) [16] and summarized in Fig. 6. The basic idea is similar to an approximate method long used in I-beam sections: that is, that warping torsion is resisted by lateral flange bending, thus the stresses that develop due to warping torsion may be found as simple bending stresses due to lateral flange bending. For I-beams the web's contribution is typically ignored. For C-sections Winter recommended assuming $\frac{1}{4}$ of the web contributed to the flange for the purposes of determining the lateral flange bending.

As Fig. 6 illustrates the stress distribution is found by summation of the pure bending stresses (Fig. 6c) with the stresses developed due to torsion (Fig. 6e). The stresses due to torsion are found by assuming the driving torsion moment $(p \cdot e)$ is restrained by a moment couple developed in the two flanges with force $p_f = p \cdot e/h$. Where the flange (flange, lip and $\frac{1}{4}$ of the web actually) is assumed to carry the load p_f, through bending, i.e. at mid-span $\sigma_B = (p_f L^2/8)x/I_y'$ where L is the span length, I_y' is the moment of inertia of the flange, lip and $\frac{1}{4}$ of the web about a y-axis through its own centroid, and x is the distance from that centroid to any part of the flange, lip, and $\frac{1}{4}$ of the web. One final step, consistent with Winter [15], but not discussed in [16] is that the uniform stress gradient on the web is ignored in favor of a linear stress gradient that connects the stresses at the two flanges at their respective flange/web junctures. Comparison of Winter's approximate method with Vlasov's theory, and shell element based finite element analysis in ANSYS [17], for the same cross-section as Fig. 5, is provided in Fig. 7. An excellent agreement is observed.

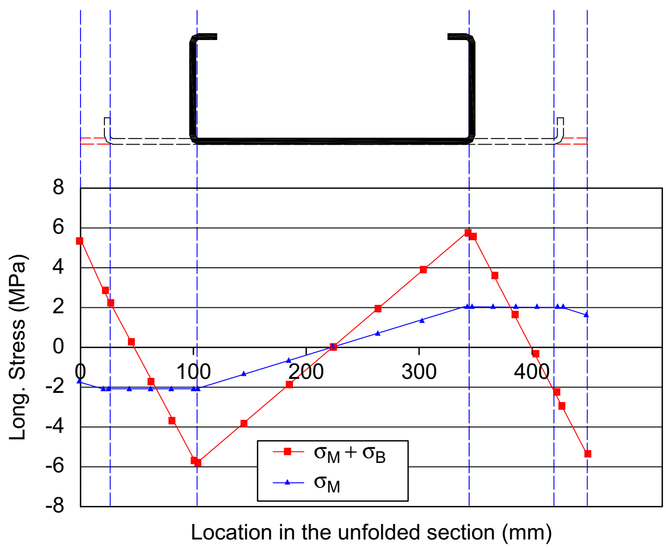

Fig. 5. Cross-section longitudinal stress distribution at mid-span (C $250 \times 85 \times 25 \times 2$, uniform load ($p$) of 0.02 N/mm, span = 7524 mm).

6. Tension flange braced: longitudinal stress demands

Winter's model provides a convenient means to understand the impact of pure bending and pure warping torsion on an unbraced, in-plane rigid, cross-section. Winter's model shows that the impact of load location can be pronounced on the resulting cross-section. For the purlin of Fig. 1, the sheeting provides restraint, but only to the tension flange, and the cross-section is thin enough that distortion is possible. Using shell element based finite element models in ABAQUS [18] (Fig. 2), we examined the longitudinal stresses at mid-span for four cases: (a) load through the flange, but otherwise "no restriction", (b) load through the flange and the sheeting provides a "rotational spring", (c) load through the flange and the sheeting provides a "rotational spring+lateral restraint", and (d) load through the flange, and lateral restraint provided in "both flanges" as shown in Fig. 8.

If both flanges are restrained, the fully braced pure bending stresses ($\sigma = My/I$) results. If both flanges are free and the load is applied to the flange the pure bending plus pure warping torsion stresses result. If a small rotational restraint is added to the

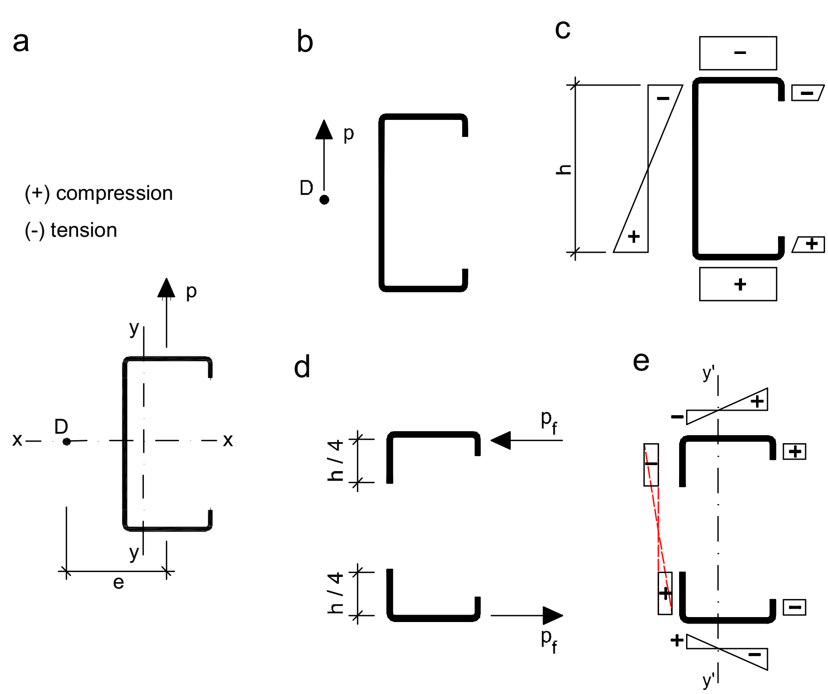

Fig. 6. Winter's model for bending and torsion in a C-section. (a) Load applied at a distance e from the shear center, (b) Load applied at the shear center (D), (c) Pure bending stress distribution, (d) Idealized section, and (e) Stress distribution at the idealized section.

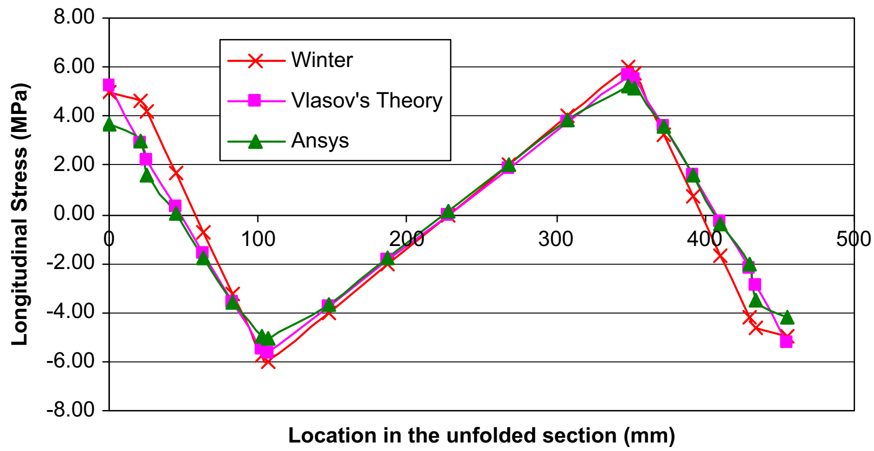

Fig. 7. Comparison of different models for torsion and bending (C 250 × 85 × 25 × 2, uniform load (p) of 0.02 N/mm, span = 7524 mm).

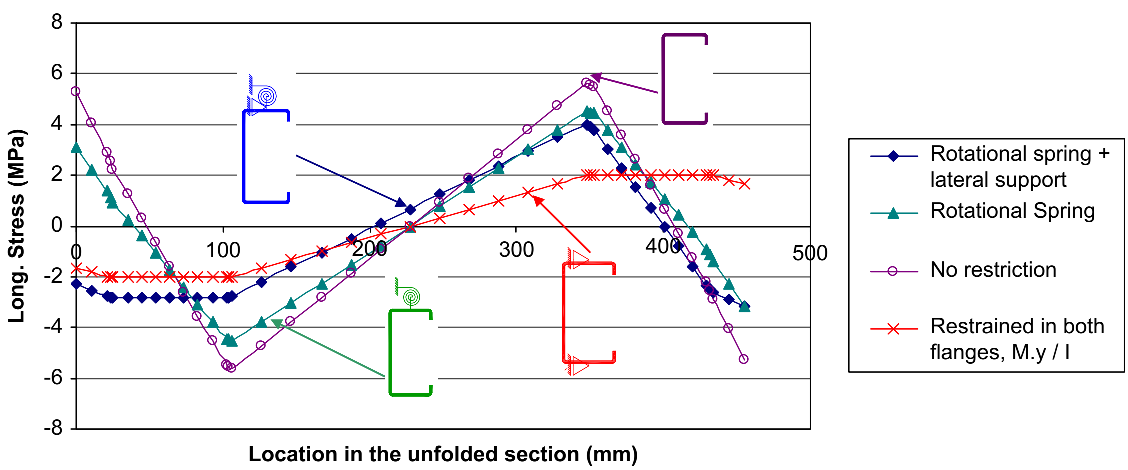

Fig. 8. Stress distribution for different kind of connections (C 250 × 85 × 25 × 2 uniform load (p) of 0.02 N/mm, span = 2052 mm).

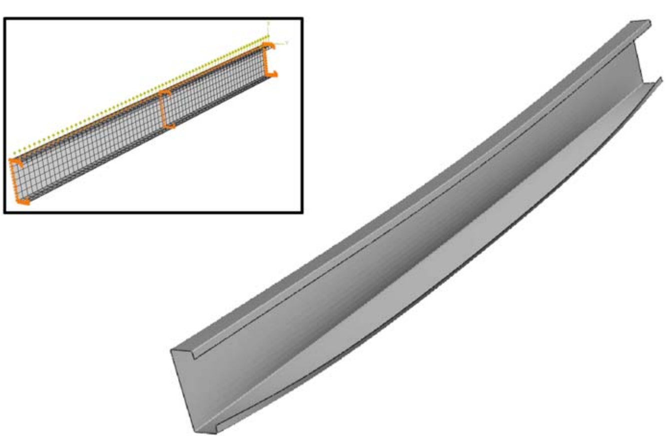

Fig. 9. Cross-section distortion associated with linear elastic deformations of a tension flange restrained purlin under uplift, ends are fully simply supported.

tension flange, the stresses due to warping torsion are decreased modestly. If full lateral support is also provided to the tension flange, the stresses and their distribution change dramatically. With the lateral restraint in place the tension flange stresses follow a pure bending distribution (but elevated from $\sigma = My/I$) while the compression flange stresses follows a reduced version of the bending plus torsion distribution.

Looking more closely at case c, where it is assumed that the sheeting can provide full lateral restraint and partial rotational restraint to the tension flange, Fig. 9 provides the linear elastic displaced shape. The key feature of the deformations is that the cross-section distorts, and as shown in the stress demands, one is left with a combination primarily of bending in the tension flange and bending plus warping torsion in the compression flange. Based on this observation a modification to Winter's model to determine the stresses when tension flange restraint is present is developed.

7. Tension flange braced: extending Winter's model

In this section Winter's model for determining the longitudinal stresses (Fig. 6) is extended to the specific case of a C-section in bending with tension flange restraints. The tension flange restraint consists of full lateral restraint and a rotational spring. The basic concept of the proposed model is provided in Fig. 10. The stresses due to pure bending (σ_M) are assumed as before, the stresses due to torsion (σ_B) are modified to provide an appropriate solution for the case where lateral tension flange restraint exists. In that case, warping and its associated stresses are assumed to concentrate in the compression flange; further the entire web height (as opposed to $\frac{1}{4}$ of the web) are assumed to participate in resisting the lateral flange bending, as illustrated in Fig. 10d–f. The rotational spring influences strongly whether σ_M or σ_B is

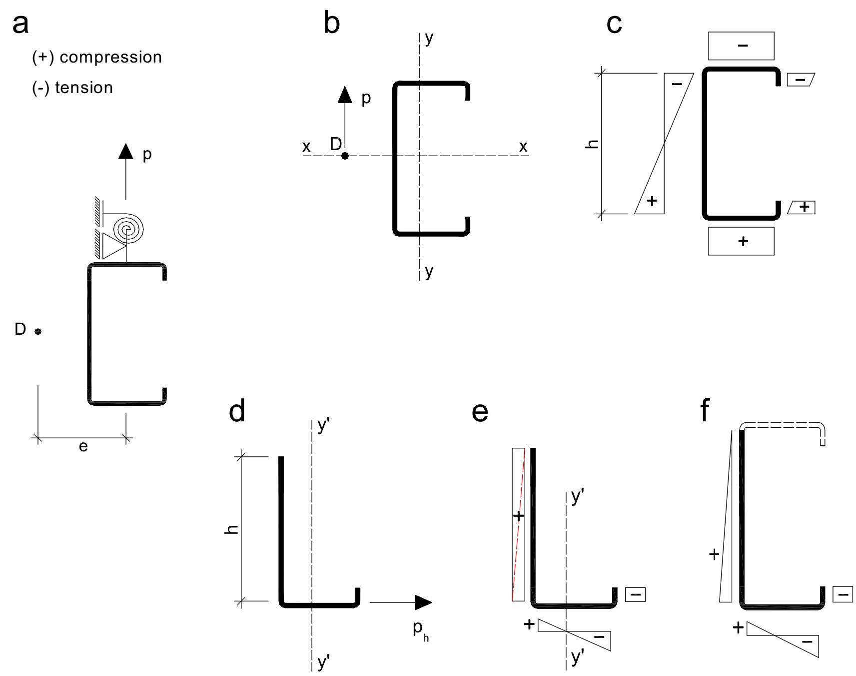

Fig. 10. Proposed model for bending and torsion with tension flange restraint. (a) Load applied at a distance e from the shear center, (b) Load applied at the shear center (D), (c) Pure bending stress distribution, (d) Idealized section, (e) Stress distribution at the idealized section, and (f) Stress distribution to be superposed.

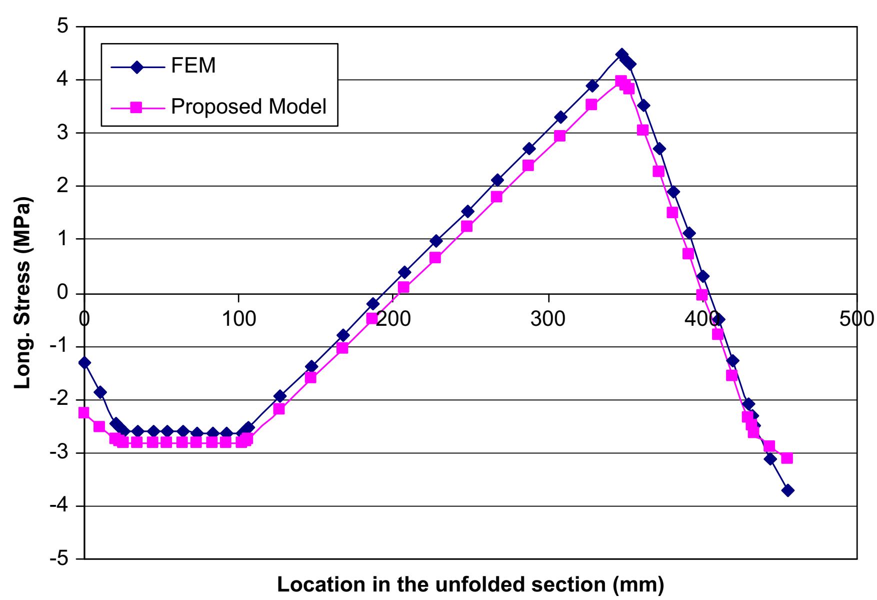

Fig. 11. Comparison between shell element FEM and proposed model (C $250 \times 85 \times 25 \times 2$ uniform load (p) of 0.02 N/mm, span = 7254 mm).

dominant and is captured in the coefficients σ_M and σ_B as given in Eq. (1) below.

The stresses in a C-section cross-section with tension flange restraint may be determined via:

$$\sigma = \alpha_M \sigma_M + \alpha_B \sigma_{B^*} \tag{1}$$

where, σ_M is the pure bending stress, as illustrated in Fig. 10c, σ_{B^*} the warping stresses when tension flange is laterally restrained, as provided in Fig. 10f, α_M the empirical factor to account for influence of tension flange rotational spring, k_{rx}, on the pure bending stress contribution, and α_B the empirical factor to account for influence of tension flange rotational spring, k_{rx}, on the stresses developed due to warping torsion.

The important feature of the above model is that it has the capability to capture stress distributions from pure bending ($\alpha_M = 1.0$, $\alpha_B = 0.0$) to partial restraint. For example, for the C $250 \times 85 \times 25 \times 2$ with a tension flange rotational spring of $k_{rx} = 0.68$ kN m/rad/m, and full lateral tension flange restraint at mid-width, the appropriate α_M and α_B are found and the resulting stress distribution from the proposed model compared with shell element based FEM is given in Fig. 11. The result shows excellent agreement with the overall distribution of stresses and good agreement with the peak stresses and stresses in the lips.

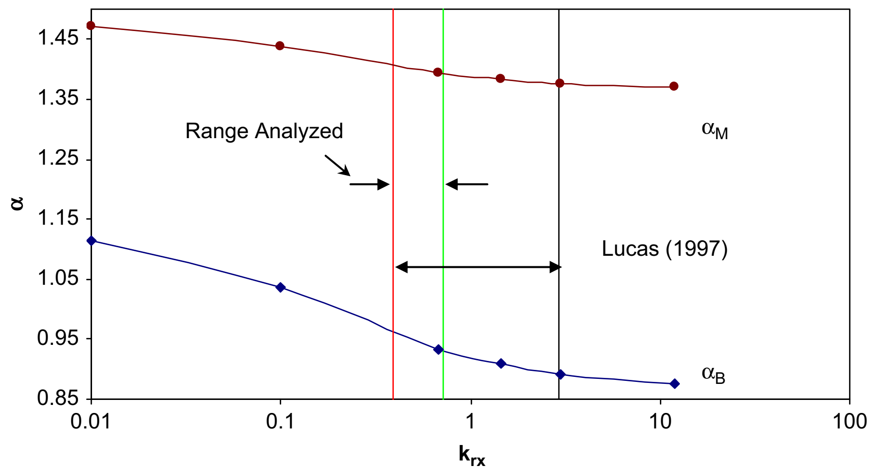

Fig. 12. Variation of α_M and α_B as a function of k_{rx} (for C $250\times85\times25\times2$, span = 7254 mm).

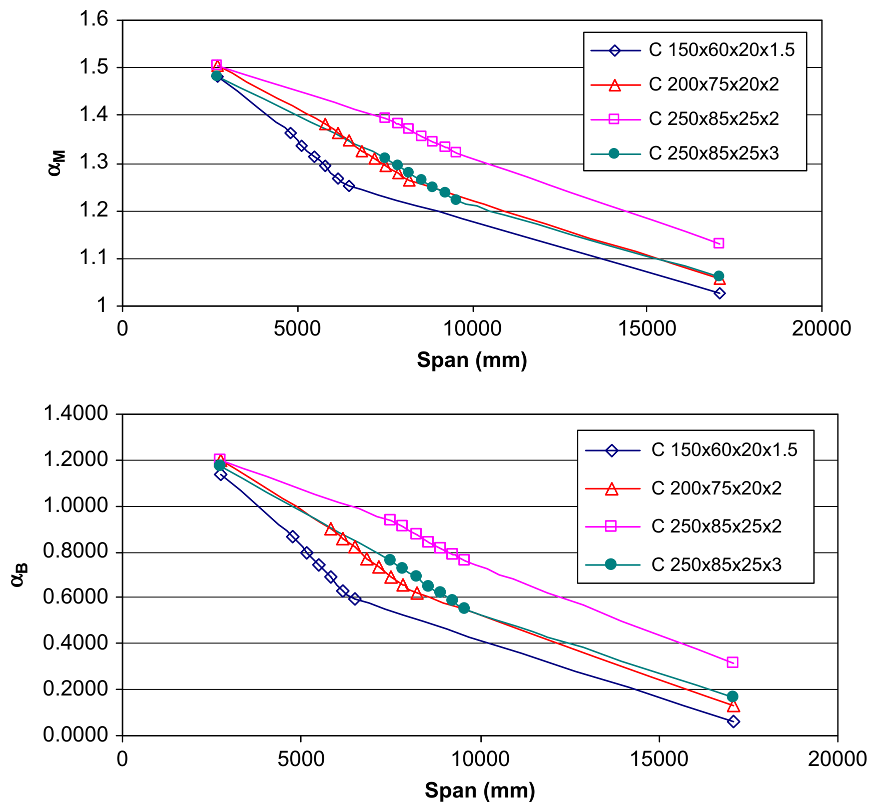

Fig. 13. Variation of α_M and α_B as a function of span length and section.

8. Study of coefficients α_M and α_B

The proposed model for predicting the stress demands in a purlin with tension flange restraint is empirical and dependent on determination of coefficients α_M and α_B. For the case of Fig. 11, α_M was found to be 1.45 and α_B to be 0.93 by minimizing the sum squared error between the model $\sigma=\alpha_M\sigma_M+\alpha_B\sigma_{B^*}$ and the finite element results (at the node locations of the FE model). The fact that α_M is greater than 1.0 does not imply that more "moment" M has been applied to the cross-section, but rather the amount which α_M is above 1.0 reflects the impact of the torsion on this tension flange restrained section. Thus, the contribution due to bending may be recognized as $1.0\sigma_M$ and the contribution due to the restrained torsion as $0.45\sigma_M+0.93\sigma_{B^*}$.

The tension flange braced case summarized in Fig. 11 is for lateral restraint at mid-width of the flange and $k_{rx}=0.72$ kN m/rad/m, as given in Table 1. The influence of the tension flange rotational spring (k_{rx}) on the stress distribution is captured in Fig. 12 through the α_M and α_B coefficients. For practical k_{rx} values the stress distribution is only modestly changed by the rotational spring. For large k_{rx} α_M and α_B trend to constant values, but α_M does not go to 1.0 and α_B to 0.0, because the cross-section still distorts and the torsion cannot be fully restrained from the tension flange alone. For small k_{rx} α_M and α_B also become constant, in this case reflecting the influence of the lateral restraint. The limiting values of α_M and α_B are cross-section, member length, loading, and boundary condition dependent.

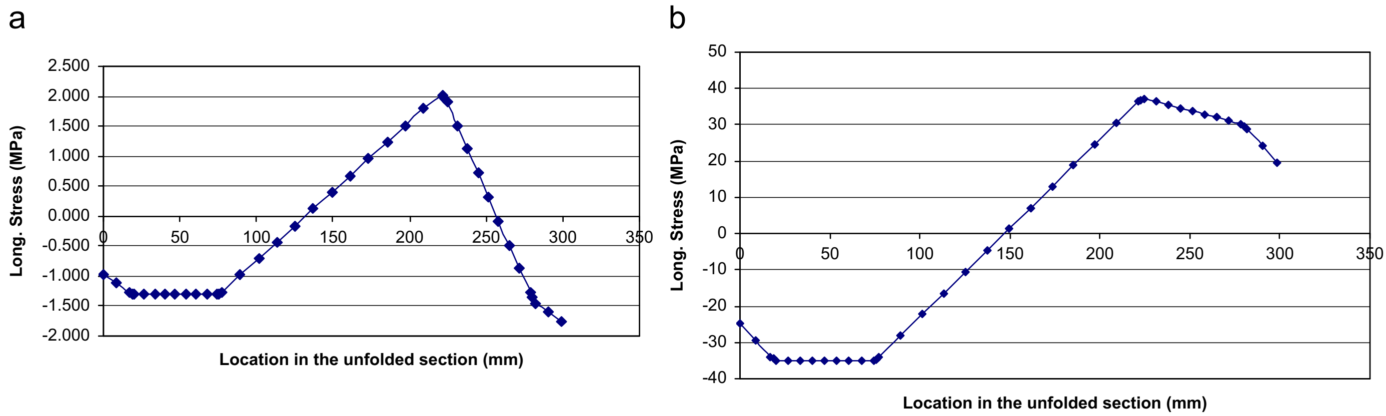

Fig. 14. Stress distribution at mid-length for C 250 × 85 × 25 × 2. (a) Span = 2.7 m and (b) span = 17.1 m.

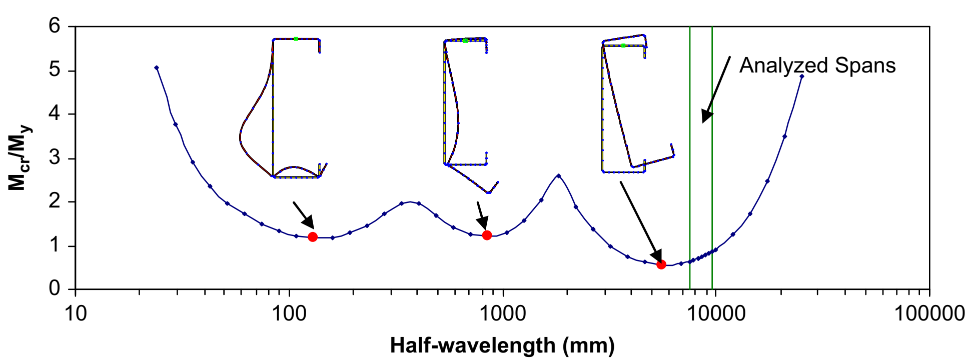

Fig. 15. Finite strip analysis for a laterally restrained C-section.

The variation of α_M and α_B for different cross-sections and span lengths are provided in Fig. 13. Over the practical range of lengths α_M and α_B vary considerably, reflecting the fact that moment ($\propto L^2$) and bimoment (torsion) vary differently as a function of length. However, despite this variation the limiting values of α_M and α_B for short span length are essentially cross-section independent; and independent of k_{rx}. For long span lengths α_M approaches 1.0 and α_B approaches 0.0, but as Fig. 13 shows, and Fig. 14 more directly indicates, even at impractically long span lengths the pure bending case is still not quite reached.

9. Design methods: AISI specification

Purlins with tension flange restraint are a longstanding problem in cold-formed steel design. In AISI-S100-07 [1] such purlins are designed per Section D6.1.1, or by testing. Section D6.1.1 defines the nominal capacity in bending, M_{nR}, as:

$$M_{nR} = R_D S_e F_y \tag{2}$$

where, R_D is a reduction factor based on the depth of the beam and falls between 0.4 and 0.7, S_e is the effective section modulus (determined based on pure bending stress) and accounts for local buckling, and F_y the yield stress.

In 2007, AISI-S100 adopted a new method, Section C3.6, to account for the influence of torsional stresses on section capacity. While the method is specifically excluded from purlins with tension flange restraint (due to the existence of Section D6.1.1) it is included here to understand better this important case. The C3.6 method uses a similar format as D6.1.1, where the nominal capacity, M_{nT}, is defined as:

$$M_{nT} = R_T S_e F_y \tag{3}$$

The reduction factor, R_T, is the ratio of the bending stress to the combined bending plus warping stress at the location of maximum combined stress; i.e. if (x^*, y^*) is the location in the cross-section where $\sigma(x^*, y^*) = \max|\sigma_M + \sigma_B|$, then for an unbraced section:

$$R_T = \sigma_M(x^*, y^*)/[\sigma_M(x^*, y^*) + \sigma_B(x^*, y^*)] \tag{4}$$

Further, if (x^*, y^*) is at the web/flange juncture R may be increased by up to 15%, but not to exceed 1.0.

10. Design methods: extending direct strength method

In the direct strength method the nominal moment capacity, M_n, is defined through a series of expressions that may be summarized functionally as:

$$M_n/M_y = f(M_{cr\ell}/M_y, M_{crd}/M_y, M_{cre}/M_y) \tag{5}$$

where the functions (f) are given in Appendix 1 of AISI-S100, and $M_{cr\ell}/M_y$, M_{crd}/M_y, and M_{cre}/M_y are the elastic local, distortional, and global buckling moments normalized by the moment at first yield, M_y. If one analyzes the stability of the section assuming $\sigma = M_y/I$ ($\alpha_M = 1.0$, $\alpha_B = 0.0$) as is common, but with the tension flange restraint in place, the results for typical cross-section stability using CUFSM [19] are provided for the C 250 × 85 × 25 × 2 section in Fig. 15. The first two minima

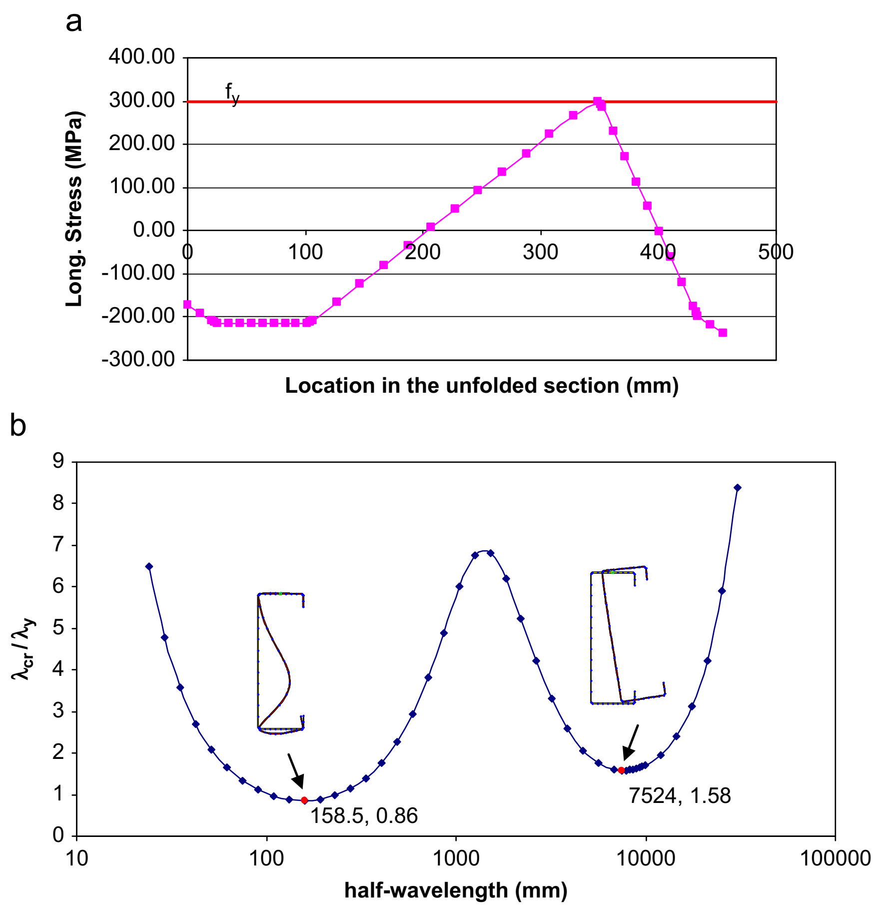

Fig. 16. Applied stress and finite strip analysis of C 250 × 85 × 25 × 2 at a span of 7524 mm. (a) Stress distribution caused by p, scaled to first yield and (b) finite strip analysis results under stress distribution of (a), note distortional buckling is indistinct, but at high enough load factors to be safely ignored.

Table 2
Comparison of design methods.

Section	Span (m)	AISI D6.1.1		AISI C3.6		Direct strength method		M_{nDSM2}/S_eF_y
						$\sigma = 1.0\sigma_M$	$\sigma = \alpha_M\sigma_M + \alpha_B\sigma_B$[a]	
		R_D	M_{nR} (kN m)	R_T[a]	M_{nT} (kN m)	M_{nDSM1} (kN m)	M_{nDSM2} (kN m)	
150 × 60 × 20 × 1.5	4.8	0.7	4.26	0.70	4.26	4.45	2.92	0.48
	6.5			0.76	4.63		3.35	0.55
200 × 75 × 20 × 2	5.8	0.65	8.69	0.71	9.49	9.02	6.14	0.46
	8.2			0.77	10.29		7.33	0.55
250 × 85 × 25 × 2	7.5	0.4	7.86	0.71	13.95	11.70	8.14	0.41
	9.6			0.74	14.54		8.74	0.44
250 × 85 × 25 × 3	7.5	0.4	12.17	0.74	22.52	17.64	14.83	0.49
	9.6			0.79	24.04		15.38	0.51

[a] 15% increase for max stress at web/flange juncture not applied.

indicate $M_{cr\ell}/M_y = 1.18$, and $M_{crd}/M_y = 1.20$, while the third minima is an unusual feature of including the restraint in the finite strip model, and is a form of restrained lateral-torsional buckling often referred to as lateral-distortional buckling ($M_{cre}/M_y = 0.56$).

Inherent in the DSM expressions and the preceding stability analysis is the assumption that only pure bending exists in the cross-section. As previously shown herein, this is not the case. How can the DSM moment expressions be extended to cover this case? To extend DSM it is proposed that the elastic stress distribution on the section with the maximum combined stresses be employed for determination of local, distortional, and global buckling.

The first step is to determine when first yield occurs, for a given pressure, p, the stress is determined and the values scaled such that $\sigma(x^*, y^*) = F_y$, as shown in Fig. 16a, for one of the C-sections studied herein. The pressure corresponding to this stress distribution is termed p_y. Next perform the cross-section stability analysis with the applied stress distribution defined by p_y[2] and determine $p_{cr\ell}/p_y, p_{crd}/p_y$, and p_{cre}/p_y as shown in Fig. 16b. These non-dimensional ratios replace the M ratios in all of the DSM

[2] In addition to including the reference applied stress $\sigma = \alpha_M\sigma_M + \alpha_B\sigma_{B^*}$, the lateral restraint and rotational spring, k_{rx}, at mid-width of the tension flange are also included. Thus, the finite strip model is an attempt to model the complete system, under its expected nonlinear stress distribution.

equations and provide a prediction of the capacity. For the simply supported case, and given the distributed load along the purlin, p, the distributed load p_n is converted back to moment M_n via:

$$M_n = p_n \ell^2/8 \quad (6)$$

thus providing a prediction for the moment that the member will carry (in the presence of that moment plus associated bimoment from the loading).

11. Comparison with design methods

The design methods are compared for the sections, restraint, and span lengths of Table 1 and provided in Table 2. The R-factor method of AISI D6.1.1 provides a reduction in the strength as the section depth increases. This reduction (R_D) does not follow the same trend as the ratio of maximum bending stress to maximum combined stress (R_T). Both of the AISI methods use local stability under the pure bending stress (i.e., that is what S_eF_y is a measure of) and ignore the actual state of stress in their attempt to empirically correct the strength.

The importance of considering stability for the actual combined stress is highlighted by the results of Figs. 15 and 16b, and shown to impact the strength significantly in Table 2 for the DSM solutions. Another interesting feature of including the actual combined stress is that strength is predicted to increase with span length. This counter-intuitive result occurs because the bimoment has less influence on the stress at longer lengths; a fact also reflected in R_T. To readily compare DSM under the combined stresses with the AISI methods M_{nDSM2} is divided by S_eF_y to provide an equivalent prediction for "R" in the final column of Table 2. The DSM method predicts that span length is more important than section depth, and shows smaller variation in predicted R.

12. Future research

Generalization of the method (α_M, α_B) for determining stress demands with tension flange restraint is needed. In particular, partial lateral restraint needs to be accounted for, as does varying member end conditions (i.e., presence or lack of anti-roll clips). Extension of the design method comparison to a greater number of sections and comparison to experimental capacities is also needed.

13. Conclusions

When singly symmetric sections are used as bending members they may be subjected to relatively complex combined longitudinal stresses due to the presence of bending and warping torsion. For the specific case of a member with bracing and loading along the tension flange, Winter's approximate method is empirically extended to predict the combined stresses. These combined stresses have a significant impact on the stability and strength of the member, as illustrated through a novel extension of the direct strength method for the design of members under such combined stresses. Work remains to generalize the proposed methods and compare with available experiments.

Acknowledgements

The authors are indebted to USIMINAS and to CNPq (Conselho Nacional de Desenvolvimento Científico e Tecnológico) (Brazil) for the grants awarded. The work reported herein was conducted by the first author as part of his master's thesis at Universidade de São Paulo under Prof. Malite's guidance and during a two months stay at Johns Hopkins University as a visiting student scholar.

References

[1] AISI-S100. North American Specification for the Design of Cold-formed Steel Structural Members. American Iron and Steel Institute, Washington, DC, 2007.
[2] Schafer BW. Review: the direct strength method of cold-formed steel member design. Journal of Constructional Steel Research 2008;64(7/8):766–78.
[3] Basaglia CD. Sobre o comportamento estrutural de terças de aço considerando a interação com as telhas—in Portuguese, (Behavior of purlin-sheeting systems). Dissertation (Master), Universidade de São Paulo, São Carlos. 2004.
[4] Sears JM, Murray TM. Proposed method for the prediction of lateral restraint forces in metal building roof systems. In: Annual Stability Conference Proceedings, Structural Stability Research Council, 2007.
[5] Seek MW, Murray TM. Lateral brace forces in single span Z-section roof systems with interior restraints using the component stiffness method. In: Annual Stability Conference Proceedings, Structural Stability Research Council, 2007.
[6] Clarke MJ, Hancock GJ. Purlin design to AISI LRFD using rational buckling analysis. In: Proceedings of the 15th International Specialty Conference on Cold-formed Steel Structures, 2000.
[7] Papangelis JP, Hancock GJ, Trahair. Computer design of cold-formed C- and Z-section purlins. Journal of Constructional Steel Research 1998;46(1–3): 169–171.
[8] Quispe L, Hancock GJ. Direct strength method for the design of purlins. In: Proceedings of the 16th International Specialty Conference on Cold-formed Steel Structures, 2002. pp. 561–72.
[9] Rousch CJ, Hancock GJ. Determination of purlin R-factors using a non-linear analysis. In: Proceedings of the 13th International Specialty Conference on Cold-formed Steel Structures, 1996.
[10] Lucas RM, Al-Bermani FGA, Kitipornchai S. Modelling of cold-formed purlin-sheeting systems: simplified model. Thin Walled Structures 1997;27(4): 263–286.
[11] LaBoube RA, Golovin M. Uplift behavior of purlin systems having discrete braces. In: Proceedings of the 10th International Specialty Conference on Cold-formed Steel Structures, 1990.
[12] Pekoz TB, Soroushian P. Behavior of C- and Z- purlins under wind uplift. In: Proceedings of the 6th Internationall Specialty Conference on Cold-formed Steel Structures, 1982.
[13] Vieira Jr., LCM. Análise numérica do comportamento estrutural e da resistência de terças de aço restringidas pelas telhas—in Portuguese, (Numerical Analysis of cold-formed steel purlin-sheeting systems). Dissertation (Master), Escola de Engenharia de São Carlos — Universidade de São Paulo, São Carlos, 2007.
[14] Vlasov VZ. Thin-walled elastic beams. Trad. Y. Schechtman (Israel Program for Scientific Translation, Jerusalem). 2 edition Washington: published for the National Science Foundation. 1961.
[15] Winter G, Lansing W, McCalley RB. Performance of Laterally Loaded Channel Beams. Four papers on the performance of thin-walled steel structures, Cornell University, Engineering Experiment Station, Reprint No. 33, 1950.
[16] AISI. North American Specification (NAS). Supplement to the North American specification for the design of cold-formed steel structures, Washington, DC, American Iron and Steel Institute; 2004.
[17] ANSYS. User's guide for revision 5.5. Houston. v.1. 1997.
[18] ABAQUS. ABAQUS/Standard Version 6.7-1, Dassault Systèmes, 〈http://www.simulia.com/〉, Providence, RI. 2007.
[19] Schafer BW, Adany S. Buckling analysis of cold-formed steel members using CUFSM: conventional and constrained finite strip methods. In: Proceedings of the 18th International Specialty Conference on Cold-formed Steel Structures, 2006. pp. 39–54.